Journal of Radioanalytical and Nuclear Chemistry (2022) 331:4047–4054
https://doi.org/10.1007/s10967-022-08454-3

Immobilization of uranium tailings by phosphoric acid-based geopolymer with optimization of machine learning

Tianji Zhao[1] · Haoyang Wu[1] · Junjie Sun[1] · Xinhai Wen[1] · Jie Zhang[1] · Weihao Zeng[1] · Hao Shen[1] · Zhitao Hu[3] · Pingping Huang[1,2]

Received: 13 May 2022 / Accepted: 17 July 2022 / Published online: 11 August 2022

Abstract

To decrease the contaminant leaching and radon exhalation from uranium tailings, a phosphoric acid-based geopolymer (PAG) precursor was selected as a solidifying agent to bind coarse sands to achieve compact structures. Machine learning was applied to explore the optimal ratio of geopolymer preparation, aimed at achieving a higher compressive strength of solidified bodies. Results showed that the maximum compressive strength of 18.964 MPa appeared at the mass ratio of 2.8 for phosphoric acid/kaolin. The uranium leaching rate of 0.70×10^{-6} cm/d on the 42nd day was three orders of magnitude less than the clay mixture-based geopolymer solidified bodies. The successful synthesis of geopolymer was evidenced by the X-ray diffraction (XRD) and Fourier transform infrared spectroscopy (FTIR), the homogeneous and dense structure of solidified bodies was characterized by the scanning electron microscopy (SEM).

Keywords Phosphoric acid-based geopolymer · Uranium tailings · Machine learning

Introduction

As a radioactive residue from mining and smelting of uranium mines, typical environmental problems arising from uranium tailings are radon emanation and contaminants leaching, including radionuclides, heavy metals and arsenic, into surface and groundwater. Among a range of technical measures that can be employed to prevent or reduce the extent of these processes, solidification technology is effective in isolating the uranium mill tailings from the outside environment [1]. For uranium mill tailings such a low-level radioactive waste, cement has been widely applied because of the low cost, easy handling and the ability to meet stringent processing and performance requirements [2]. Nevertheless, cement curing-based solidification is constrained due to its shortcoming of volume increase, intensive energy consumption, time-consuming and massive CO_2 emission [3–5]. Therefore, exploring alternative materials with clean, low carbon and high efficiency has been an urgent necessity.

Geopolymerrization is a kind of technology to convert activated aluminosilicate sources such as metakaolin, which featured by rich in silica (SiO_2) and alumina (Al_2O_3), by the basic or acidic attack at low temperature into geopolymer. It has been seen as the third generation cement after lime and ordinary Portland cement [6]. Besides as a cement replacement, geopolymers have been applied to encapsulate toxic and radioactive wastes due to certain advantages such as curing efficiency, mechanical strength, freeze-thaw resistance, heat resistance, and durability. For instance, the Pb(II), Cu(II), Cd(II) and Cr(III) immobilized properties by kaolin and zeolite-based geopolymer were investigated. It exhibited lower energy and cost-consuming than the metakaolin-based geopolymer immobilization, and a lower leaching rate than the previous works for metakaolin and fly ash-based geopolymers [7]. In the study by Xu and co-workers, the performance of cement and metakaolin-based geopolymer to immobilize strontium were compared [8]. It revealed that the denser microstructure of metakaolin-based geopolymer and the geopolymer solidified blocks exhibited better leaching

✉ Pingping Huang
huangpingping@usc.edu.cn

1 School of Resource Environment and Safety Engineering, University of South China, Hengyang 421001, Hunan, China

2 Hunan Province Engineering Technology Research Center of Uranium Tailings Treatment, Hengyang 421001, Hunan, China

3 College of Mechanical Engineering, University of South China, Hengyang 421001, Hunan, China

resistance and stable compressive strength than cement solidified blocks. Moreover, Huang's group proposed the utilization of geopolymer for heavy metal immobilization in the lead-zinc tailing [9]. The coal gangue and blast furnace slag were used as the raw materials to synthesize composite geopolymer, and the compressive strength of solidified bodies with 70% leading-zinc tailings reached 21.68 MPa.

In an attempt to examine the feasibility of geopolymer as uranium tailings solidifying agent, the phosphoric acid-based mechanical activated kaolin was selected to prepare a geopolymer precursor. On the one hand, the phosphoric acid-based geopolymer shows superior properties than the alkali-activator geopolymer [10]. On the other hand, mechanically activated kaolin is an aluminosilicate produced from the grinding of kaolin, exhibiting to be more reactive than thermally activated kaolin [11]. Compared to the heat treatment of kaolin, the mechanically activated kaolin would decrease the use of fossil fuels and the release of CO_2, NO_x and SO_x. In addition, to produce denser microstructures in the solidified bodies, sintering steps were conducted, avoiding the tediously curing time of 28 days [12, 13].

As the major performance index of solidified bodies, the compressive strength is significantly affected by the ratio of raw materials [14]. However, single-factor experiment and orthogonal experiment are limited by their subjectivity and inherently defects thus be labor-intensive and time-consuming to exhaust all ratios. In sharp contrast, the machine learning algorithm can fully exploit the feature information hidden in multidimensional data and transform it into the desired mathematical model after learning and processing, so as to apply it in various fields. Recently, Yang and co-workers combined the artificial neural network and a genetic algorithm to predict the operating parameters disposal of real rolling wastewater, indicating the feasibility of machine learning in waste treatment [15].

Herein, preparation of mechanical activated kaolin-based geopolymer with rational raw material design and solidification of uranium mill tailings were conducted in this study. The relationship of variables (i.e., phosphoric acid concentration, water content) and compressive strength of solidified body was explored by the particle swarm optimization-support vector machine (PSO-SVM). The leaching test and radon exhalation measurement were carried out to evaluate the solidification efficiency of uranium tailings with PAG. Furthermore, the XRD, FTIR and SEM were used to provide insight into PAG's work forms and mechanisms.

Table 2 The mass ratio of raw materials

Group number	Mass ratio (Kaolin: DI water: Phosphoric acid solution) (g)
G1	40:60:32
G2	40:60:38
G3	40:60:44
G4	40:60:50
G5	40:60:52
G6	40:60:58
G7	40:60:64
G8	40:60:70
G9	40:60:76
G10	40:60:82
G11	40:60:88
G12	40:60:94
G13	40:60:100
G14	40:60:106
G15	40:60:112
G16	40:60:118
G17	40:60:124

Experiment

Experimental materials

The uranium tailings are all from a uranium tailing impoundments in south China. The kaolin is obtained from a kaolin mine in southwest China. The concentrated phosphoric acid solution is purchased from Aladdin (AR, ≥ 85 wt % in H_2O, concentration of 14.614 mol/L). The particle size distribution of uranium tailings is mainly coarse sand with 0.5 mm, all uranium tailings were dried at 105 °C for 24 h to remove moisture contents. The kaolin was dried at 60 °C, while the mechanical treatment of the kaolin was conducted using the YXQM-2L type planetary ball mill. The dried kaolin sample was put in the agitated tank with a capacity of 500 cm^3 using agate balls with different dimensions, and kaolin with a particle size of 0.075 mm was obtained. The chemical composition of kaolin is shown in Table 1.

Table 1 The chemical composition of kaolin (wt %)

SiO_2	Al_2O_3	K_2O	TiO_2	Fe_2O_3	MgO	P_2O_5	Na_2O	CaO	SO_3	Cr_2O_3
55.05	40.02	1.71	1.42	0.99	0.27	0.14	0.08	0.04	0.04	0.02

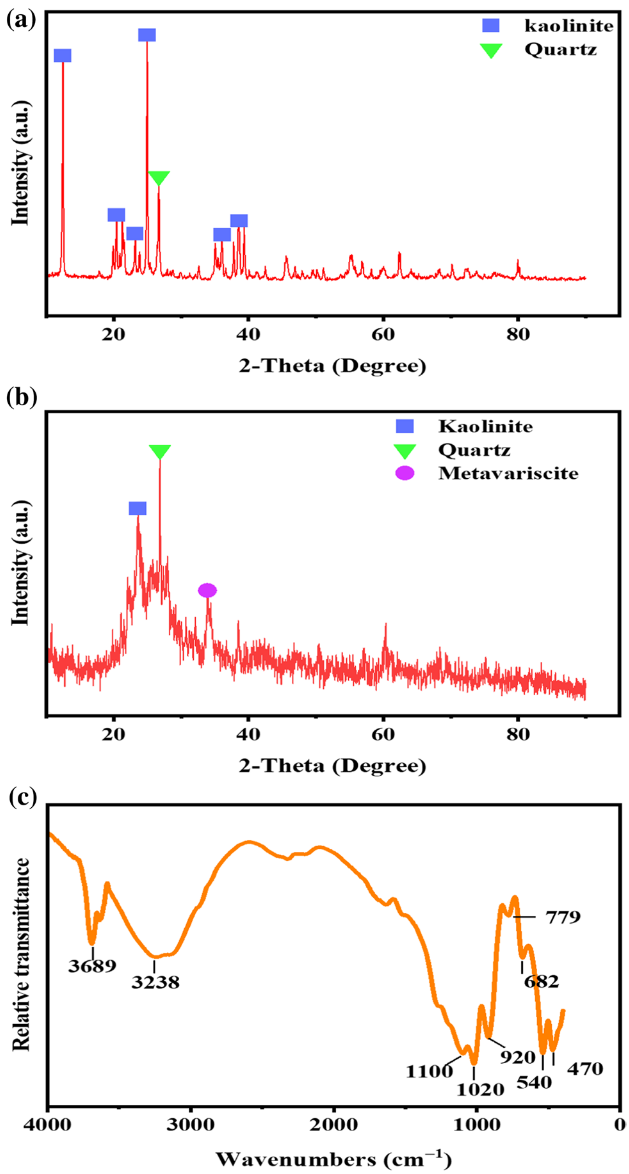

Fig. 1 **a**, **b** XRD pattern of kaolin and PAG with raw material ratio of G16. **c** FTIR spectra of the PAG with raw material ratio of G16

Geopolymer synthesis

In order to synthesize an appropriate geopolymer precursor that can successfully stabilize the uranium tailings, geopolymer samples with various raw materials mass ratios, as listed in Table 2 were prepared. In the synthesis sequence, the kaolin suspension was mixed with the phosphoric acid solution at 90 °C for 100 min with magnetic stirring. When the solution turned white, the phosphoric acid-based geopolymer (PAG) was obtained.

Uranium tailings solidification with PAG

Upon the addition of 105 g PAG onto 305 g uranium tailings, the mixtures were prepared in a porcelain mortar until the paste was homogeneous. Then the mixture was taken into a metal mould and uniaxially pressed at 150 MPa to form cylindrical compacts with a diameter of 50 mm and a height of about 80 mm. The uranium tailings solidified bodies bound by PAG was obtained after 30 min of calcination at 800 °C in the air atmosphere.

Characterization test

The Fourier Transform Infrared Spectrometer (FTIR, IRA-1S WL) was used to determine the functional group and chemical bond in the PAG. The X-ray diffraction patterns of the kaolin and PAG were collected, and the mineral phases were identified. The morphology of the solidified specimen was observed by scanning electron microscope (SEM, TESCAN MIRA LMS).

The uniaxial compressive strength test of Φ 50 × 80 mm solidified bodies was conducted according to the standard GB/T 17,671–2021 and GB 14,569.1–2011. The RAD7 Electronic Radon Detector was used to determine the radon exhalation of solidified bodies, and the calculation formula was as follows:

$$J = \frac{K \cdot V_e}{S} \tag{1}$$

where J is the Radon exhalation rate on one side of solidified body, in $Bq \cdot \mathrm{m}^{-2} \cdot \mathrm{s}^{-1}$; K is the slope of the one-side fitting curve of the accumulated radon concentration of the solidified body, in $\mathrm{Bq} \cdot \mathrm{m}^{-3} \cdot \mathrm{s}^{-1}$; S is the single exposed base area of the solidified body, in m^2; V_e is the effective volume in radon collecting space except for solidified bodies, m^3.

The leaching test was conducted according to the China standard GB/T 7023—2011. The DI water with pH = 7.0 was chosen as the leaching solution, and the prepared uranium tailings solidified bodies were completely immersed in the 500 mL experiment devices. The supernatant was extracted at 1 d, 3 d, 7 d, 14 d, 21 d, 28 d, 35 d, and 42 d. The uranium concentration was analyzed by an inductively coupled plasma (ICP) mass spectrometer (MS). The leaching rate and cumulative amount of leaching of uranium were calculated following the equation:

$$R_n = \frac{a_n/A_0}{(S/V)(\Delta t)_n} \tag{2}$$

$$P_t = \frac{\sum a_n/A_0}{S/V} \tag{3}$$

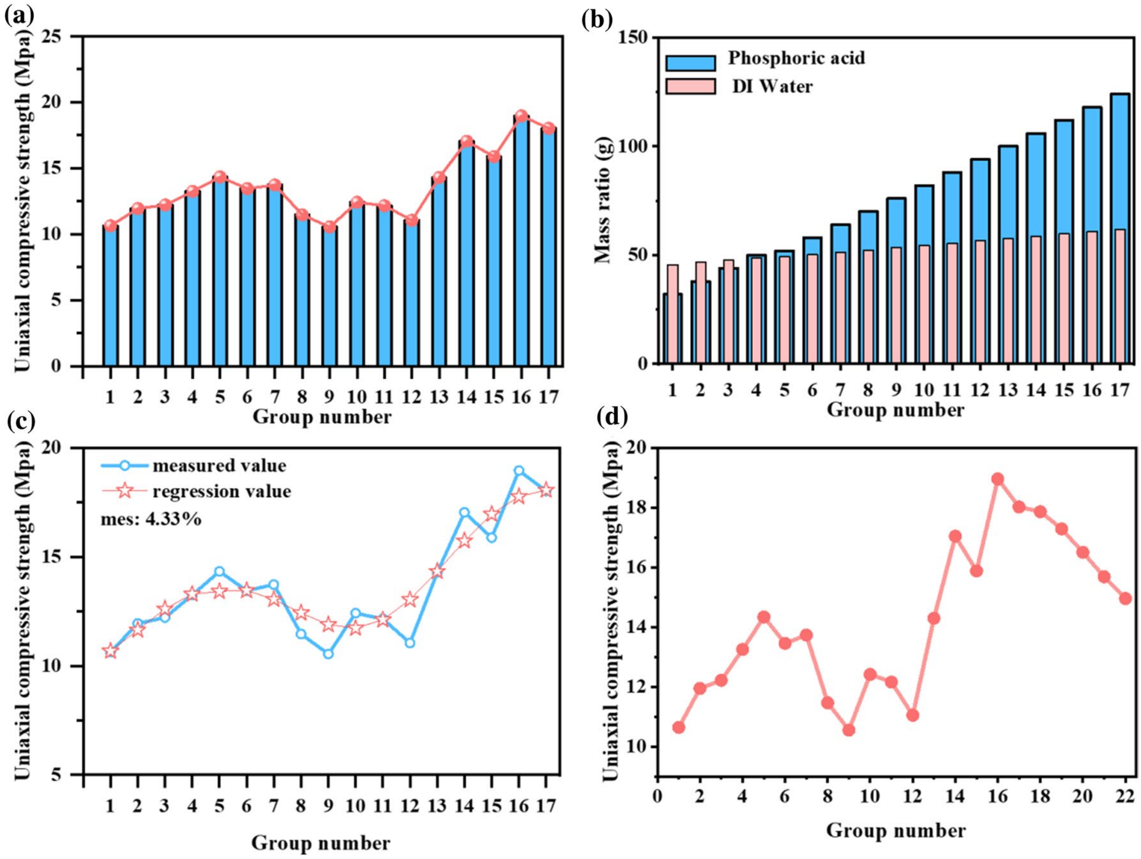

Fig. 2 **a** The compressive strength curve of PAG solidified uranium tailings. **b** The mass ratio of phosphoric acid/DI water. **c** The measured compressive strength and fitting regression results from the PSO-SVM model. **d** The compressive strength prediction curve of PAG solidified bodies

where R_n is the leaching rate of group i in the nth leaching cycle, in cm/d; a_n is the mass of group i solidified body in the nth leaching cycle; A_0 is the initial mass of group i in the solidified body sample; S is the contact geometric surface area between the solidified body and the leached solution; V is the volume of solidified body; $(\Delta t)_n$ is the time required for the nth leaching cycle; P_t is cumulative amount of leaching of uranium, in cm.

Results and discussion

The XRD patterns of the sample of kaolin and PAG with the raw ratio of G16 are shown in Fig. 1a and b, respectively. Figure 1a exhibits the kaolinite and quartz phase in the kaolin. After the kaolin was activated by phosphoric acid, as shown in Fig. 1b, the presence of quartz is indicated by the strongest peak at 26.8°, which does not contribute to the geopolymerization reaction [16]. The peak at 23.6° is the residual kaolinite peak with reduced intensity. Apart from this, the peak appears at 33.7°, which can be indexed to metavariscite ($AlPO_4·2H_2O$), resulting from the reaction between the leached aluminum and the PO_4 tetrahedra of phosphoric acid. Significantly, the broad and diffuse peak from 17.9° to 32.9° is considered the amorphous phase in PAG [17]. The metavariscite phase and the diffuse halo demonstrate the successful synthesis of PAG. The FTIR spectra in Fig. 1c schematically illustrates the existence of various chemical bonds of PAG. As shown in Fig. 1c, the bands at 3689 cm^{-1}, 3238 cm^{-1} and 540 cm^{-1} are the consequences of unreacted kaolin in the product of PAG [17]. The bands at 470 cm^{-1} and 779 cm^{-1} are related to Si–O–Si bending vibration, corresponding to stretching vibration and in-plane bending vibration, respectively [18, 19]. The main band at 682 cm^{-1} is attributed to Al–O–P symmetric stretching vibration [19], while the peaks at 1020 cm^{-1} and 920 cm^{-1} are considered as P–O stretching asymmetric vibrations of [PO_4]. Apart from this, the band that appears at 1100 cm^{-1} is assigned to the O–P–O vibration corresponded to [PO_4] [20, 21].

As shown in Fig. 2a, the compressive strength values of the solidified bodies display irregular changes but generally increase with the rise of the phosphoric acid solution ratio and reaches a peak at 18.964 Mpa, which was in accordance with the Chinese standards GB 14,569.1–2011 (no less than

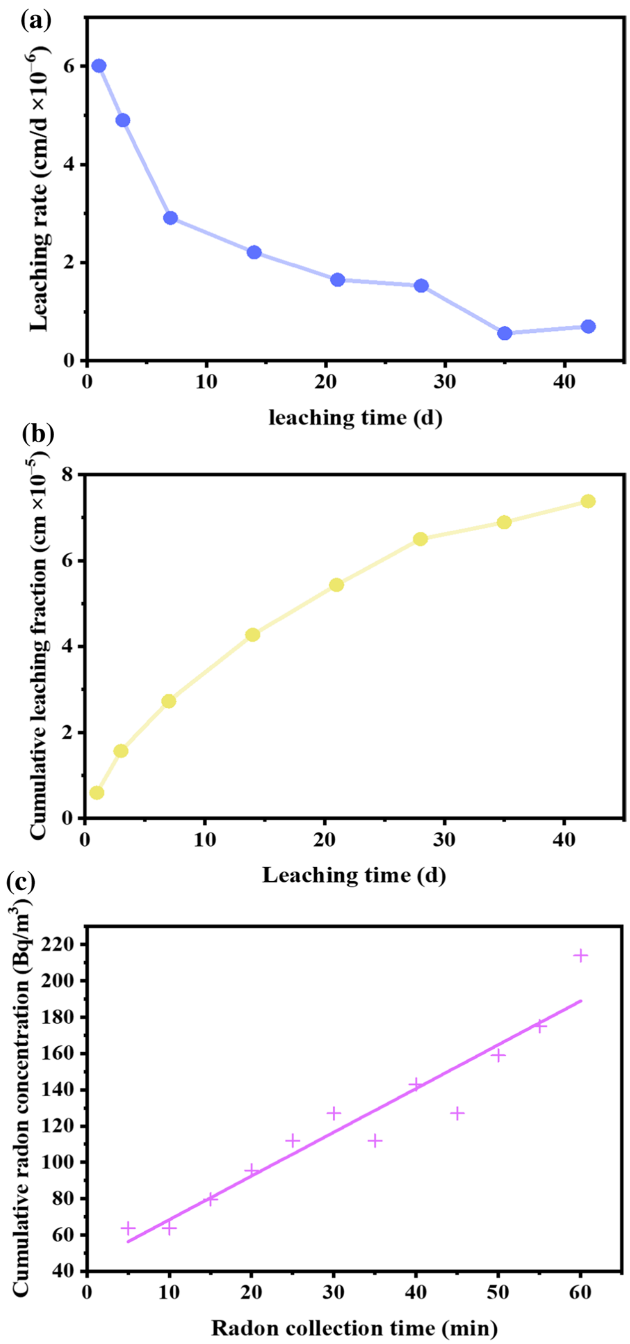

Fig. 3 **a** The leaching rate and **b** cumulative leaching fraction of uranium in uranium tailings solidified with PAG in raw material ratio of G16. **c** The fitted curve of cumulative radon concentration of uranium tailings solidified with PAG in raw material ratio of G16

7 Mpa). A leading cause of irregular change in compressive strength is the concentration variation of the phosphoric acid solution, which means the simultaneous mass change of phosphoric acid and water (Fig. 2b). Samet and co-workers revealed that the reaction mechanism of phosphoric acid-based geopolymer is H^+ destroys Al-O bond in kaolin, and then $[PO_4]$ tetrahedron reacts with Al^{3+} and kaolin to form $AlPO_4$ and Si–O–P bonds, finally [Si–O–P] polycondensation forms a new three-dimensional network structure [16]. Therefore, the molar ratio of P/Al is vital for the preparation of phosphoric acid-based geopolymer, which means the high or low content of phosphoric acid will result in an excessive reaction and incomplete reaction, respectively. Specifically, originating from a dearth of H^+ at a low proportion of phosphoric acid content will result in the inadequate dissolution of Al and subsequent incomplete reaction that reduces the compressive strength; while at a high proportion of phosphoric acid content, superfluous PO_4^{3-}, HPO_4^{2-}, $H_2PO_4^-$ will be consumed by metal ions to balance the charge and cause a reduction in geopolymer. Apart from this, the compressive strength is also correlated with a water content that affects the dissolution of Al^{3+} in kaolin and the accumulation of heat during the preparation reaction [22–24]. Therefore, the rational design of phosphoric acid and water content ratio is of great significance to the excellent mechanical property of PAG solidified bodies.

The compressive strength curve of solidified bodies with irregular variation delivered a complex nonlinear relationship between raw material mix ratio and compressive strength. It is formidably difficult for orthogonal design to comprehensively analyze the insight link between the content of raw material ratio and strength properties. The support vector machine (SVM) is an efficient algorithm to solve complex nonlinear problems, with the main features of small data volume requirement, low algorithm complexity and high-performance computing. The core idea of SVM is the map the nonlinear low-dimensional sample data into the linear high-dimensional space through the kernel function, so that the relationship between the data becomes linear and the optimal global solution can be obtained theoretically [25, 26].

Based on the SVM algorithm, we constructed linear regression functions for 17 sets of sample data in high-dimensional space:

$$\mathrm{f}(\mathrm{x}) = \omega^T \varphi(x) + b \tag{4}$$

where ω is weight vector; $\varphi(x)$ is nonlinear mapping function, and b is offset vector.

The objective function and constraint condition of SVM can be described as formulas (5) and (6), respectively.

$$\min_{\omega,b,\xi} \frac{1}{2}\omega + C\sum_{i=1}^{n}(\xi + \xi^*) \tag{5}$$

$$\text{s.t.} - \left(\varepsilon + \xi_i^*\right) \le y - \omega\varphi\left(x_i\right) - b \le \varepsilon + \xi_i \tag{6}$$

where C is the penalty factor; ε is the insensitive parameter;ξ and ξ^* are slack variable.

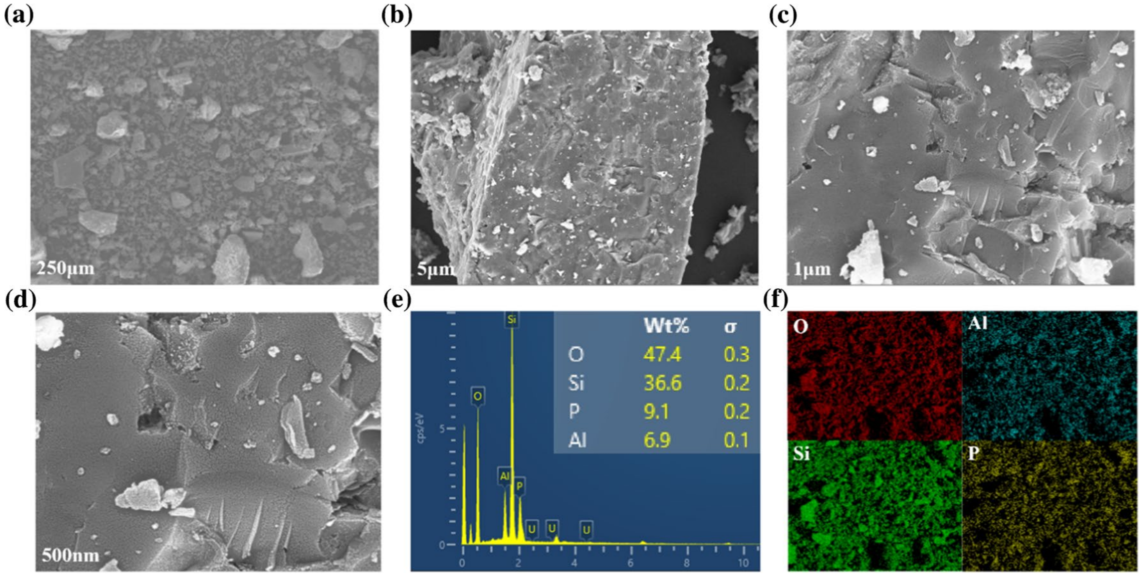

Fig. 4 **a**–**d** SEM images of uranium tailings solidified samples with PAG in raw material ratio of G16. **e** EDS spectra of **a**. **f** EDS scanning images of **a**

In order to solve Eqs. (5) and (6), the Lagrangian function is introduced to transform it into a dual optimization problem and the radial basis function is chosen for the kernel function. The formula can be described as:

$$\mathrm{f}(x) = \omega^{*}\varphi(x) + b^{*} = \sum_{i=1}^{L}\left(\alpha_i - \alpha_i^{*}\right)K\left(x_i, x_j\right) + b^{*} \tag{7}$$

$$K\left(x_i, x_j\right) = \exp\left(-\frac{\| x - x_i \|}{2g^2}\right) \tag{8}$$

Therefore, the penalty factor C and the kernel function parameter g are involved in the algorithm's calculation. Establishing a precise SVM model requires the determination of reasonable parameters C and g, the particle swarm optimization (PSO) is chosen to optimize parameters [27, 28]. PSO is inspired by the predation behavior of birds, the process of PSO can be described as setting a swarm of random particles firstly, then the optimal solution is obtained by constantly updating the optimal position of all particles through iteration. The core formula of PSO can be expressed as:

$$v_i^d = \omega v_i^{d-1} + c_1 r_1\left(pbest_i^d - x_i^d\right) + c_2 r_2\left(gbest^d - x_i^d\right) \tag{9}$$

$$x_i^{d+1} = x_i^d + v_i^d \tag{10}$$

where v is the particle velocity; ω is the inertia weight; c_1 and c_2 are the learning factor; r_1 and r_2 are the random numbers on [0,1].

Taking the 17 groups of experiments data as training sets to form an accurate PSO-SVM model, meantime imports the forecast ratio of phosphoric acid and DI water to calculate the strength variation tendency of solidified bodies. As shown in Fig. 2c, the fitted regression curve is basically coincident with the original strength curve and the mean-square error (mse) is 4.33%, which means an accepted level. Meanwhile, it is observed that peak intensity appears at G16, subsequently the compressive strength gradually decreases with the proportion increase of phosphoric acid/DI water, indicating that the G16 experiment is the optimal mix of raw materials (Fig. 2d). Although the training sets data is limited, the accuracy of the PSO-SVM model indicates the feasibility of this method, simultaneously providing reference and guidance for the design of raw material ratio of geopolymer precursor and the research of performance optimization of dopants like polyvinyl alcohol fiber, fiberglass, and etc.

As we all know, the strength of solidified bodies is related to porosity. The smaller porosity represents the more tightly the phosphoric acid-based geopolymer binds the uranium tailings, which means better resistance performance of radionuclide leaching and radon exhalation rate of solidified bodies. Therefore, the radon exhalation rate and uranium leaching were measured for the solidified tailings at a G16 ratio of phosphoric acid to DI water. The leaching rate and accumulative leaching fraction of uranium in solidified bodies are shown in Fig. 3a and b, respectively. As shown in Fig. 3a, the curve of the leaching rate gradually decreases and tends to be stable after 28 d. The leaching rate of PAG solidified uranium tailing on the 42nd day is 0.70×10^{-6} cm/d, which is much lower than alkali-activator geopolymer solidified bodies of 0.29×10^{-3} cm/d, 1% polyvinyl alcohol (PVA) fibers doped geopolymer solidified bodies of 0.393×10^{-3} cm/d and 1% basalt fibers doped geopolymer solidified bodies of 0.323×10^{-3} cm/d [29]. The results revealed the exceptional nuclide packaging performance of PAG solidified bodies. As shown in Fig. 3b, the cumulative leaching fraction of uranium increases gradually and tends to level off at 42 d with 7.38×10^{-5} cm. The cumulative radon concentration fitted curve is displayed in Fig. 3c, and the radon exhalation rate calculated according to Eq. (1) is 0.42 Bq•m^{-2}•s^{-1}, which complies with the China standard of radiation protection in uranium mining and metallurgy (below 0.74 Bq•m^{-2}•s^{-1}) (GB 23,727–2020).

The micromorphology and the energy dispersive spectrometer (EDS) spectra of the solidified bodies with PAG in raw material ratio of G16 are shown in Fig. 4. Figure 4a, b manifested an amorphous structure of PAG solidified bodies, which also featured the heterogeneous system. In addition, the higher resolution SEM image (Fig. 4c, d) reveals the smooth surface and heterogeneous distribution of the solidified bodies. As shown in Fig. 4e, f, the EDS spectra displays that the elements of O, Si, Al and P in PAG solidified bodies are homogeneously distributed without obvious enrichment, the content of Si is the largest.

Conclusion

In this study, the solidification efficiency of mechanical activated kaolin-based geopolymer on radioactive waste i.e., uranium tailings was evaluated. The PSO-SVM model was constructed to investigate the optimal ratio of raw materials in the geopolymer precursor synthesis. Under the optimum mass ratio of phosphoric acid/kaolin as 2.8, the compressive strength of PAG solidified uranium tailings was 18.964 MPa. The leaching rate of uranium in solidified bodies was 0.70×10^{-6} cm/d after 42 days of leaching, which was three orders of magnitude lower than the leaching rate of alkali-based geopolymer immobilized uranium tailings, showing excellent performance in preventing uranium leaching. The XRD and FTIR results showed the successful synthesis of geopolymer. The SEM of solidified bodies showed the compact microstructures, which contributed to the high compressive strength and low leaching of radionuclide uranium.

Acknowledgements This work was supported by the Project Approved by the Provincial Education Department of Hunan Province, China (No.19A420), the Natural science foundation of Hunan Province (Grant Nos. 2020JJ5463; 2021JJ40463).

References

1. Liu B, Peng T, Sun H, Yue H (2017) Release behavior of uranium in uranium mill tailings under environmental conditions. J Environ Radioact 171:160–168. https://doi.org/10.1016/j.jenvrad.2017.02.016
2. Vu T, Gowripalan N (2018) Mechanisms of heavy metal immobilisation using geopolymerisation techniques – a review. J Adv Concr Technol 16:124–135. https://doi.org/10.3151/jact.16.124
3. Jiang F, Guo J, Wang X, Liu Y, Li X, Chen G, Wang Z, Yang J, Tan B (2020) Experimental study on the leaching performance of U(VI) solidified by uranium tailing cement with different admixtures and ratios. Environ Technol Innov. https://doi.org/10.1016/j.eti.2019.100506
4. Jiang F, Hao Y, Wu H, Liu Y, Wang Z, Tan B, Zhang C, Lan M (2022) Study on damage degradation and radon emission from uranium tailing polymer-solidified soil under freeze-thaw cycles. J Radioanal Nucl Chem. https://doi.org/10.1007/s10967-022-08219-y
5. Wang F, Chen G, Ji L, Yuan Z (2020) Preparation and mechanical properties of cemented uranium tailing backfill based on alkali-activated slag. Adv Mater Sci Eng. https://doi.org/10.1155/2020/6345206
6. Singh B, Ishwarya G, Gupta M, Bhattacharyya SK (2015) Geopolymer concrete: a review of some recent developments. Constr Build Mater 85:78–90. https://doi.org/10.1016/j.conbuildmat.2015.03.036
7. El-Eswed BI, Yousef RI, Alshaaer M, Hamadneh I, Al-Gharabli SI, Khalili F (2015) Stabilization/solidification of heavy metals in kaolin/zeolite based geopolymers. Int J Miner Process 137:34–42. https://doi.org/10.1016/j.minpro.2015.03.002
8. Tan Q, Li N, Xu Z, Chen X, Peng X, Shuai Q, Yao Z (2019) Comparative performance of cement and metakaolin based-geopolymer blocks for strontium immobilization. J Ceram Soc Jpn 127:44–49. https://doi.org/10.2109/jcersj2.18130
9. Zhao SJ, Xia M, Yu L, Huang X, Jiao BQ, Li DW (2021) Optimization for the preparation of composite geopolymer using response surface methodology and its application in lead-zinc tailings solidification. Constr Build Mater. https://doi.org/10.1016/j.conbuildmat.2020.120969
10. Liu LP, Cui XM, Qiu SH, Yu JL, Lin Z (2010) Preparation of phosphoric acid-based porous geopolymers. Appl Clay Sci 50:600–603
11. Derouiche R, Baklouti S (2021) Phosphoric acid based geopolymerization: Effect of the mechanochemical and the thermal activation of the kaolin. Ceram Int 47:13446–13456. https://doi.org/10.1016/j.ceramint.2021.01.203
12. Baifa Z, Guo H, Yuan P, Deng L, Zhong X, Li Y, Wang Q, Liu D (2020) Novel acid-based geopolymer synthesized from nanosized tubular halloysite: the role of precalcination temperature and phosphoric acid concentration. Cement Concr Compos 110:103601. https://doi.org/10.1016/j.cemconcomp.2020.103601
13. Chen S, Zhou Z-W, Sun X-W (2021) Immobilization of simulated 137CsCl using metakaolin based geopolymers obtained by hybrid hydrothermal-sintering processes. J Radioanal Nucl Chem 330:1285–1298. https://doi.org/10.1007/s10967-021-08048-5
14. Jiang F, Chen G, Li M, Liu Y, Li X, Guo J, Wu H, Wang Z (2019) Experimental study of different admixture effects on the properties of uranium mill tailing solidified bodies. J Radioanal Nucl Chem 322:1159–1168. https://doi.org/10.1007/s10967-019-06825-x
15. Yang Q, Xu R, Wu P, He J, Liu C, Jiang W (2021) Three-step treatment of real complex, variable high-COD rolling wastewater by rational adjustment of acidification, adsorption, and

photocatalysis using big data analysis. Sep Purif Technol. https://doi.org/10.1016/j.seppur.2021.118865
16. Louati S, Baklouti S, Samet B (2016) Acid based geopolymerization kinetics: effect of clay particle size. Appl Clay Sci 132:571–578. https://doi.org/10.1016/j.clay.2016.08.007
17. Zhang B, Guo H, Deng L, Fan W, Yu T, Wang Q (2020) Undehydrated kaolinite as materials for the preparation of geopolymer through phosphoric acid-activation. Appl Clay Sci. https://doi.org/10.1016/j.clay.2020.105887
18. Mathivet V, Jouin J, Gharzouni A, Sobrados I, Celerier H, Rossignol S, Parlier M (2019) Acid-based geopolymers: Understanding of the structural evolutions during consolidation and after thermal treatments. J Non-Cryst Solids 512:90–97. https://doi.org/10.1016/j.jnoncrysol.2019.02.025
19. Styskalik A, Skoda D, Moravec Z, Abbott JG, Barnes CE, Pinkas J (2014) Synthesis of homogeneous silicophosphate xerogels by non-hydrolytic condensation reactions. Micropor Mesopor Mater 197:204–212. https://doi.org/10.1016/j.micromeso.2014.06.019
20. Bekiaris G, Peltre C, Jensen LS, Bruun S (2016) Using FTIR-photoacoustic spectroscopy for phosphorus speciation analysis of biochars. Spectroch Acta Part A: Molecul Biomol Spectrosc. https://doi.org/10.1016/j.saa.2016.05.049
21. Jastrzębski W, Sitarz M, Rokita M, Bułat K (2011) Infrared spectroscopy of different phosphates structures. Spectrochimica Acta Part A: Molecul Biomol Spectrosc. https://doi.org/10.1016/j.saa.2010.08.044
22. Djobo JNY, Nkwaju RY (2021) Preparation of acid aluminum phosphate solutions for metakaolin phosphate geopolymer binder. RSC Adv 11:32258–32268. https://doi.org/10.1039/d1ra05433c
23. Tchakoute HK, Ruescher CH, Kamseu E, Andreola F, Leonelli C (2017) Influence of the molar concentration of phosphoric acid solution on the properties of metakaolin-phosphate-based geopolymer cements. Appl Clay Sci 147:184–194. https://doi.org/10.1016/j.clay.2017.07.036
24. Tchakoute HK, Ruescher CH, Kamseu E, Djobo JNY, Leonelli C (2017) The influence of gibbsite in kaolin and the formation of berlinite on the properties of metakaolin-phosphate-based geopolymer cements. Mater Chem Phys 199:280–288. https://doi.org/10.1016/j.matchemphys.2017.07.020
25. Liu L, Han G, Xu Z, Jiang J, Shu L, Martinez-Garcia M (2022) Boundary tracking of continuous objects based on binary tree structured svm for industrial wireless sensor networks. IEEE Trans Mob Comput 21:849–861. https://doi.org/10.1109/tmc.2020.3019393
26. Yoon S, Hyun-Tae B, Kim G-Y, Min JH (2021) Evaluation of a thermal conductivity prediction model for compacted clay based on a machine learning method (기계학습법을 통한 압축 벤토나이트의 열전도도 추정 모델 평가). KSCE J Civil Environ Eng Resear 41:123–131
27. Jin W, Zhang J-q, Zhang X (2011) Face recognition method based on support vector machine and particle swarm optimization. Expert Syst Appl 38:4390–4393. https://doi.org/10.1016/j.eswa.2010.09.108
28. Tan X, Yu F, Zhao X (2019) Support vector machine algorithm for artificial intelligence optimization. Clust Comput J Netw Softw Tool Appl 22:15015–15021. https://doi.org/10.1007/s10586-018-2490-7
29. Jiang F, Tan B, Wang Z, Liu Y, Hao Y, Zhang C, Wu H, Hong C (2022) Preparation and related properties of geopolymer solidified uranium tailings bodies with various fibers and fiber content. Environ Sci Pollut Res 29:20603–20616. https://doi.org/10.1007/s11356-021-17176-0